

# Deep Brain Stimulation

March 7, 2019

580.435/635 Applied Bioelectrical Engineering  
Prof. Leslie Tung  
Department of Biomedical Engineering  
Johns Hopkins University

1

## What you can expect to learn today

- Lead placement
- Lead configurations and designs
- Volume of tissue activated (VTA)
- Axonal stimulation
- Computational models of VTA and clinical outcomes
- DBS waveforms

2

## Understanding therapeutic merits of DBS in Parkinsonian neural networks

**Forward tilt of trunk**

**Reduced arm swinging**

**Shuffling gait with short steps**

**Rigidity and trembling of head**

**Rigidity and trembling of extremities**

**Brain Regions Affected by Parkinson's Disease**

Parkinson's disease

<http://www.medstorx.com/wp-content/uploads/2013/02/parkinsons-disease.jpg>  
<http://diseasespictures.com/wp-content/uploads/2012/11/Parkinsons-Disease->

3

## DBS Lead Placement

**a**

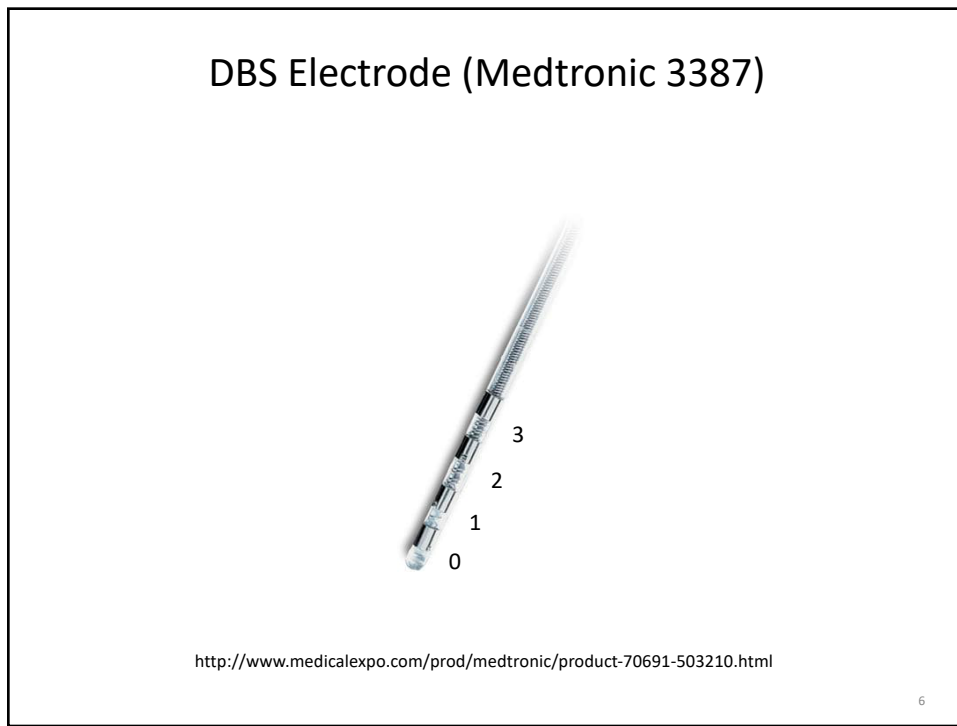
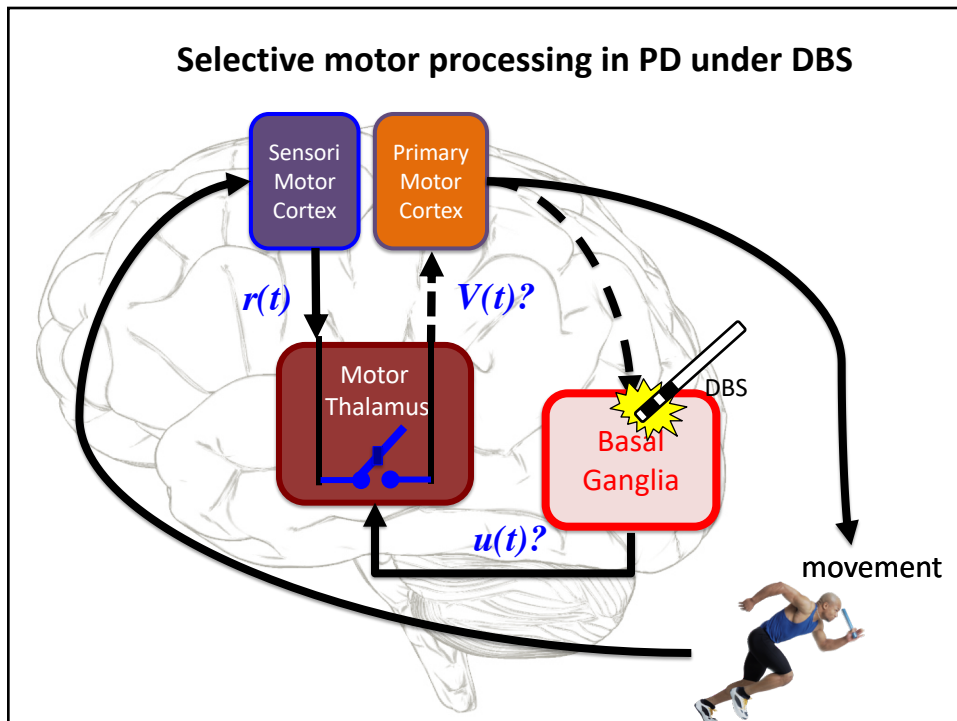
**b**

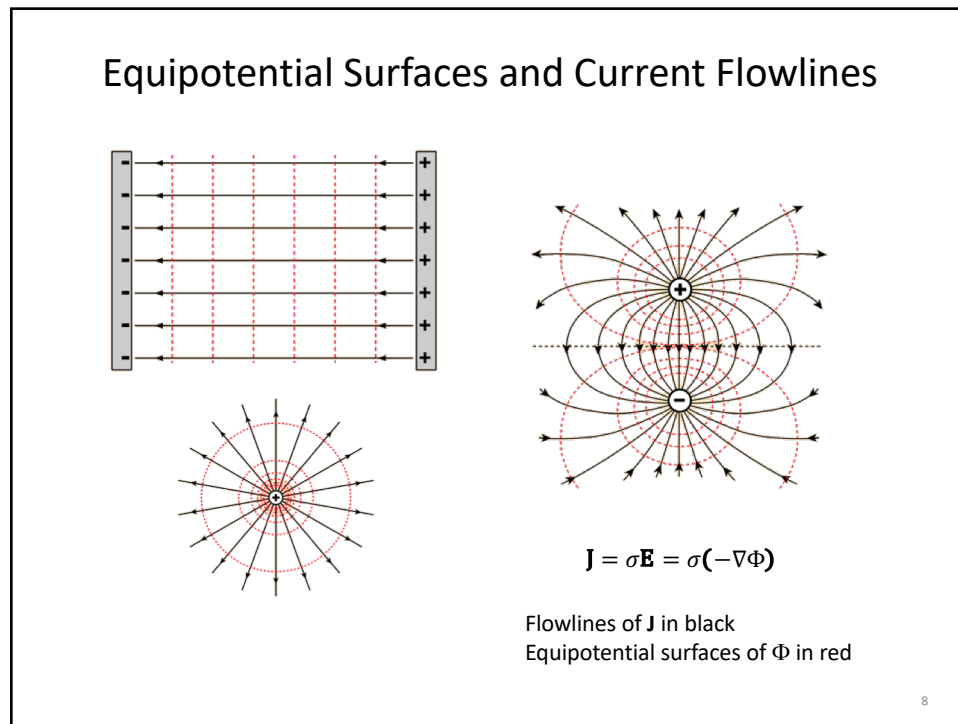
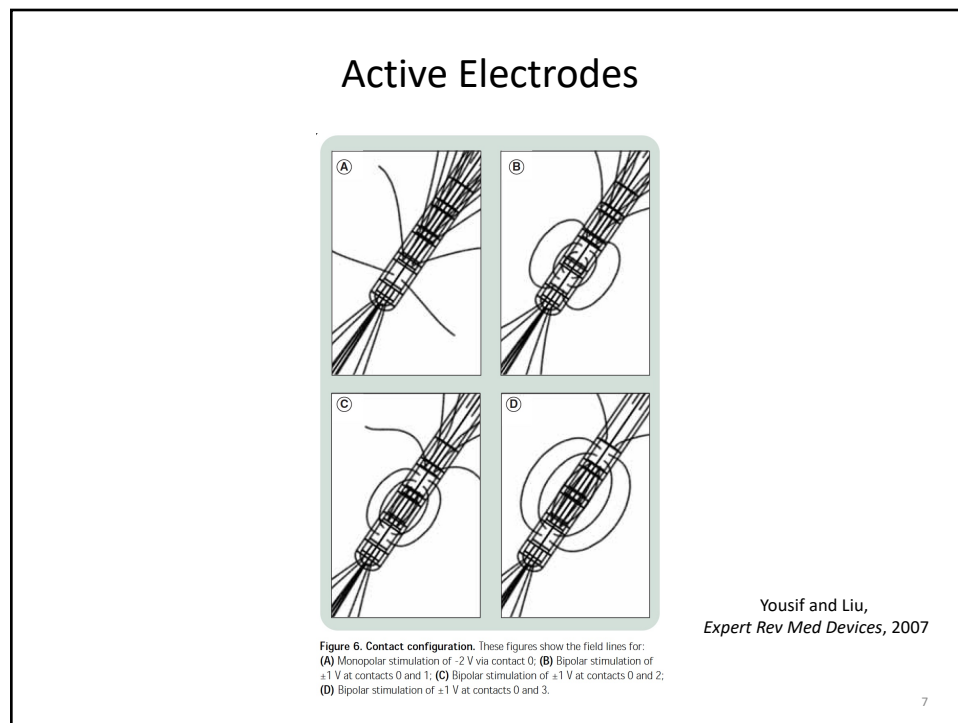
*From lecture by Dr. Sri Sarma*

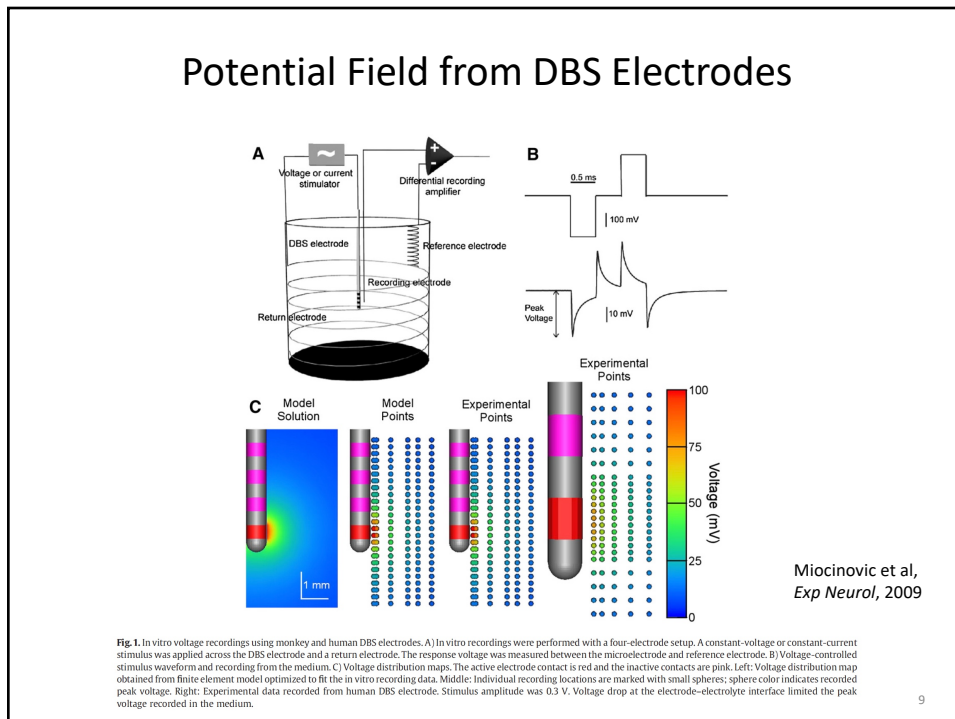
**Figure 7.** (a) Coronal magnetic resonance imaging (MRI) showing bilateral deep-brain stimulation electrodes, implanted for the treatment of Parkinson's disease. (b) Chest radiograph showing typical placement of the subcutaneously implanted stimulator hardware.

Lewis et al, *Neuroscientist*, 2016

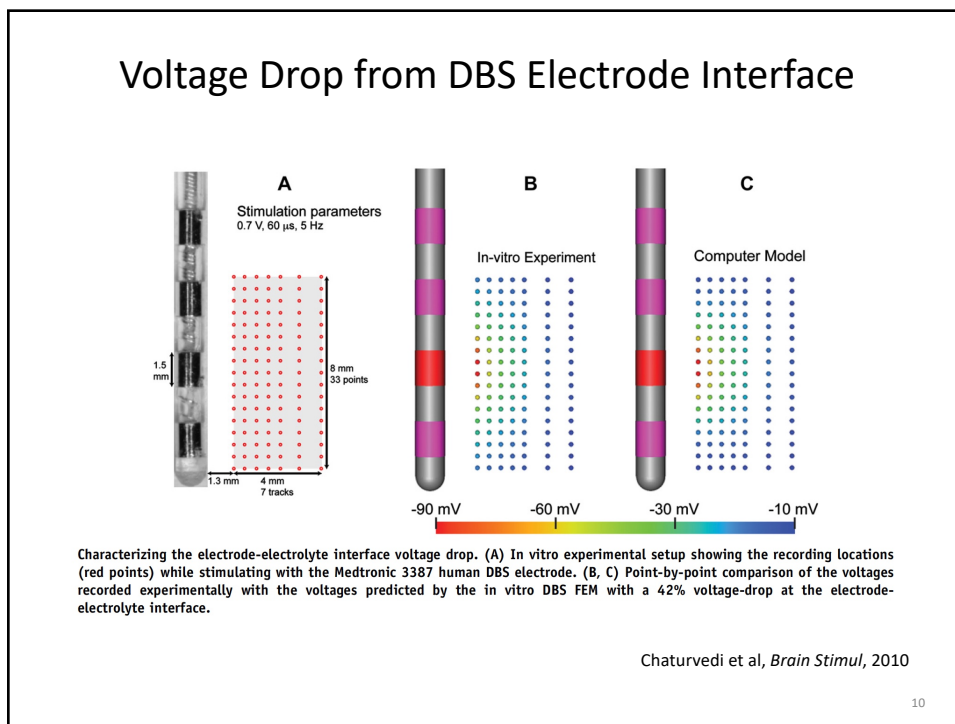
4



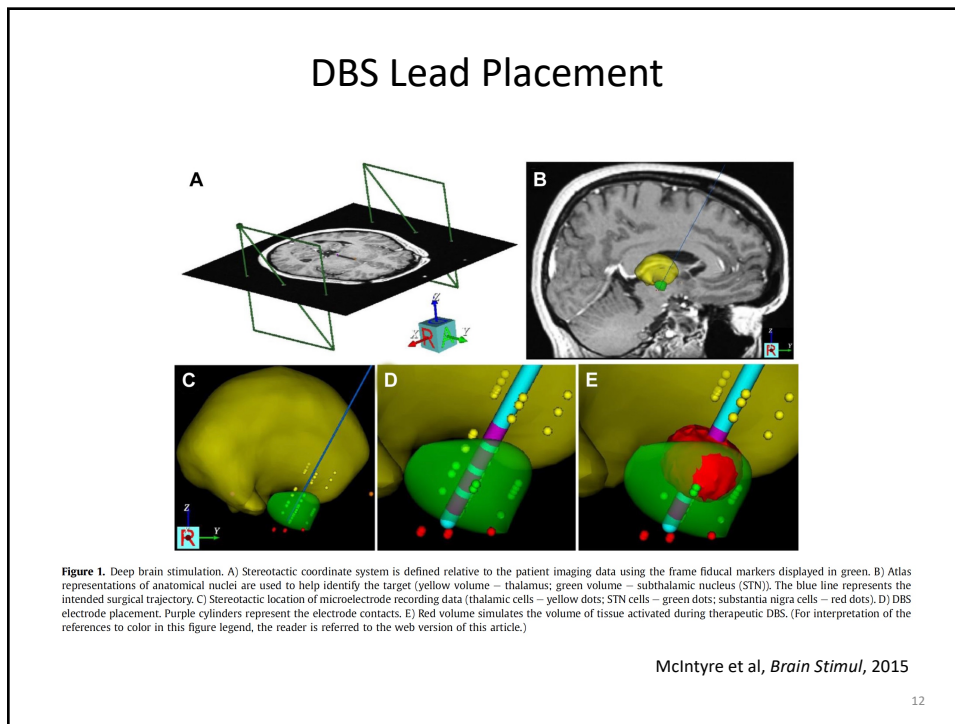
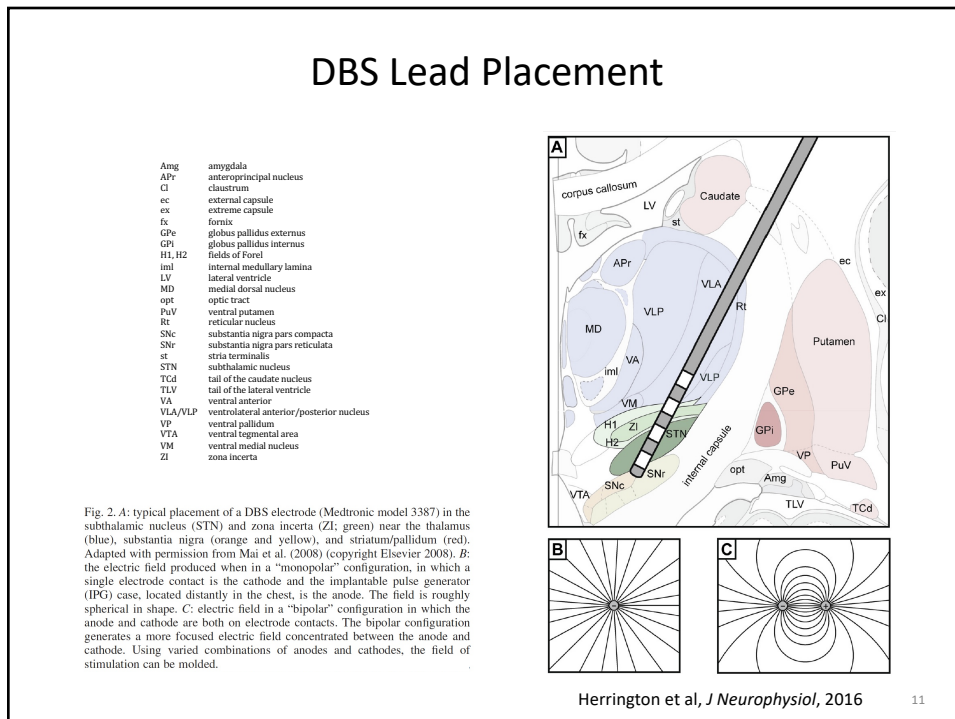


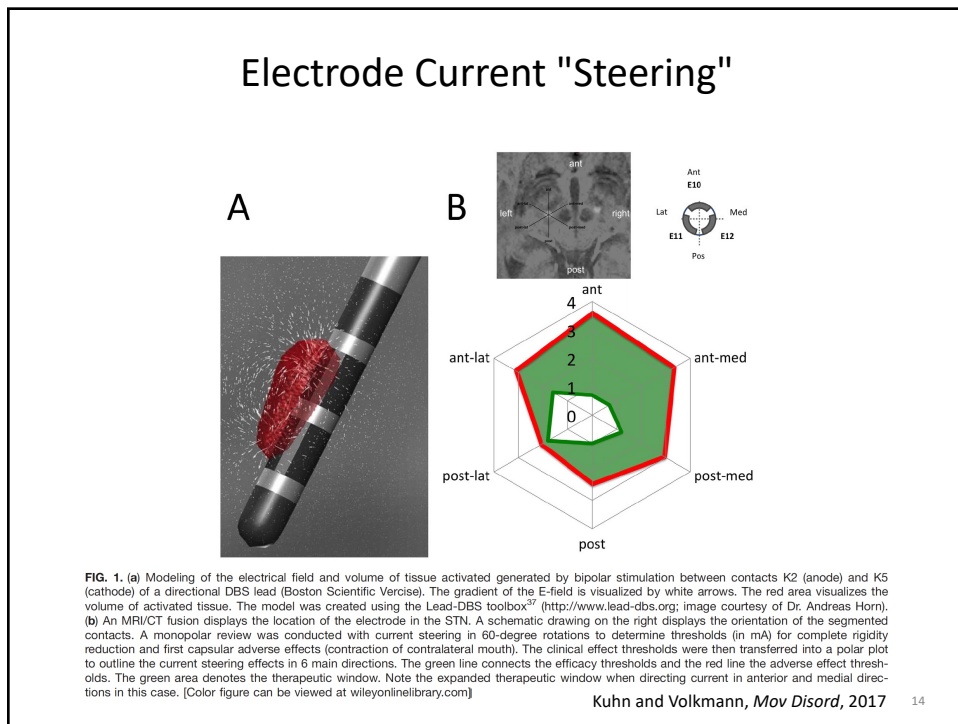
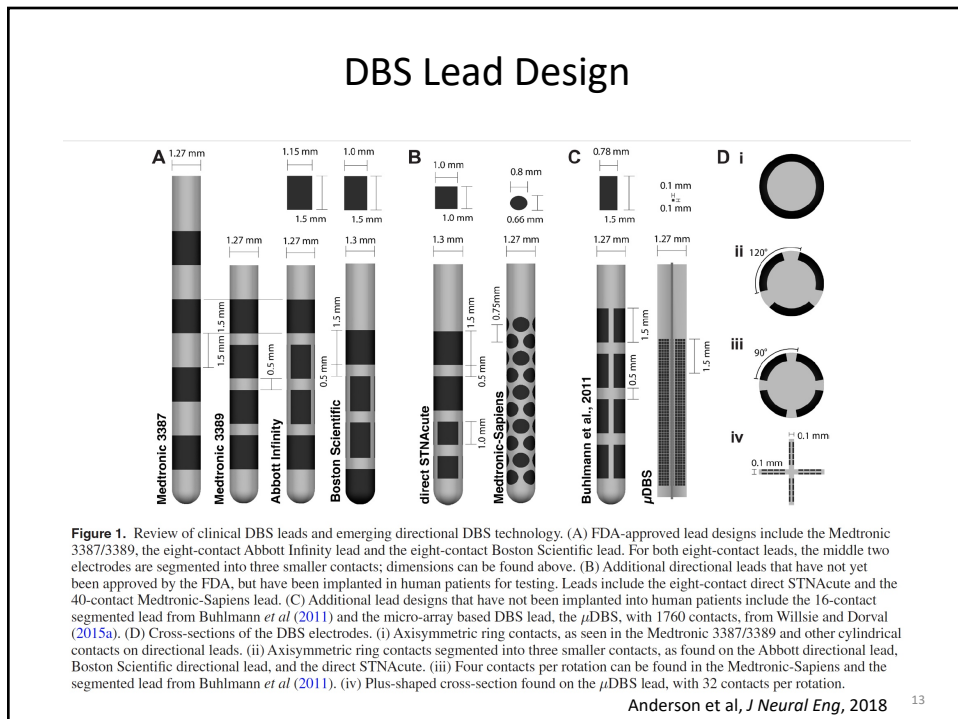


9



10





## DBS Lead Placement

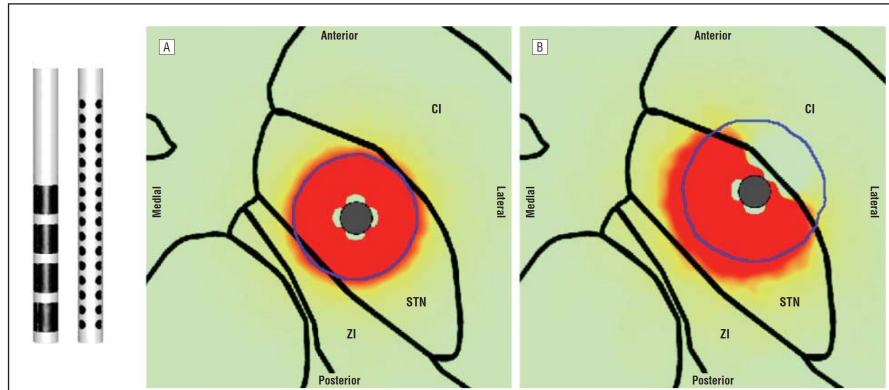


**Figure 3.** Current steering using novel deep brain stimulation (DBS) array electrode design. Estimate of volume of activated tissue is overlaid with an atlas section. A, Conventional DBS electrode (left) activates tissue contained within the blue circle, which is adequate for the electrode positioned in the center of the subthalamic nucleus (STN). B, Displacing the electrode by 1 mm laterally and anteriorly causes undesired activation of the internal capsule (CI) with the conventional electrode, but it can be avoided by using a novel DBS array electrode.<sup>88</sup> Reprinted with permission. ZI indicates zona incerta.

Miocinovic et al, *JAMA Neurol*, 2013

15

## Cathodal and Anodal Stimulation

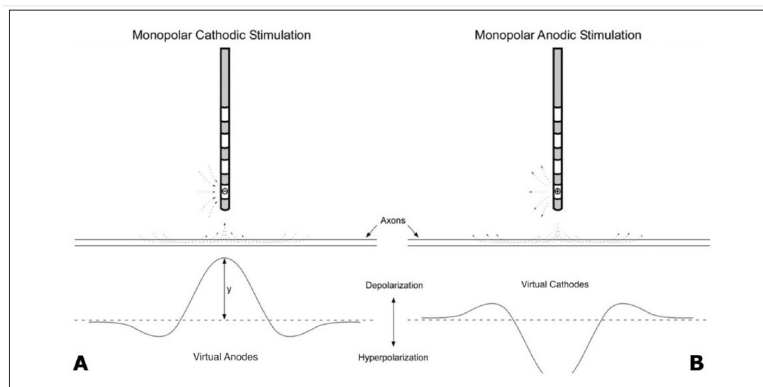


**Figure 4.** Illustration depicting cathodic versus anodic monopolar stimulation. During cathodic stimulation (A, left), current is drawn from the axon of a neuron proximal to the electrode, resulting in depolarization. This results in current being drawn into the axon from surrounding tissue distant to the electrode, hyperpolarizing the axon membrane and creating "virtual anodes" at these sites. Note however that the strength of hyperpolarization at the virtual anodes is much weaker (approximately 5 times less) than the depolarization proximal to the electrode (cathode). Thus, during anodic stimulation (B, right), the same phenomenon occurring in reverse results in remote depolarization at "virtual cathodes." Given the lower amplitude of depolarization at the virtual cathodes, a greater stimulus strength is required for this to result in neuronal firing. Note that the electrodes depicted contain multiple electrodes, thus stimulation could be performed in a bipolar fashion, with one electrode acting as the cathode, with the other as the anode. Figure adapted from Brocker and Grill (2013), with permission.

Lewis et al, *Neuroscientist*, 2016 16

## Unmyelinated and Myelinated Axons

*Rattay, IEEE Trans Biomed Eng, 1986*

Myelinated:  $C_m \frac{dV_n}{dt} + I_{ion,n} = G_a(V_{n-1} - 2V_n + V_{n+1} + V_{e,n-1} - 2V_{e,n} + V_{e,n+1})$

Unmyelinated:  $c_m \frac{dV}{dt} + i_{ion} = \frac{1}{r_i} \left( \frac{\partial^2 V}{\partial x^2} + \frac{\partial^2 V_e}{\partial x^2} \right)$

$c_m \frac{dV_n}{dt} + i_{ion,n} = \frac{1}{r_i} \left( \frac{V_{n-1} - 2V_n + V_{n+1}}{\Delta x^2} + \frac{V_{e,n-1} - 2V_{e,n} + V_{e,n+1}}{\Delta x^2} \right)$

17

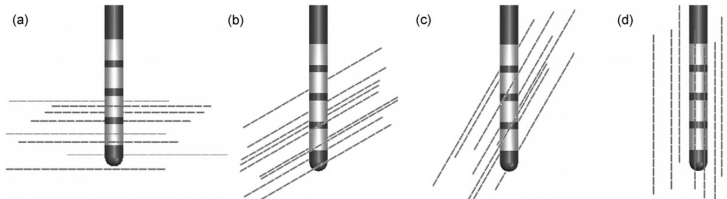
## Nerve Fiber Model

FIG. 1. Multi-compartment double cable model of a mammalian axon. The model consisted of 21 nodes of Ranvier separated by 20 internodes. Each intermodal section of the model consisted of 2 paranodal myelin attachment segments (MYSA), 2 paranodal main segments (FLUT), and 6 intermodal segments (STIN). The nodal membrane dynamics included fast (Naf) and persistent (Nap) sodium, slow potassium (Ks), and linear leakage (Lk) conductances in parallel with the nodal capacitance ( $C_n$ ). The intermodal segments were represented by a double cable structure of linear conductances with an explicit representation of the myelin sheath ( $G_m$  in parallel with  $C_m$ ) and the intermodal axolemma ( $G_i$  in parallel with  $C_i$ ).

McIntyre et al, *J Neurophysiol*, 2002

18

## Nerve Stimulation



**Figure 1.** Depictions of axon populations and electrode geometries that were tested. Axons were oriented at 90° (a), 60° (b), 30° (c) and 0° (d) with respect to the electrode axis, and axons were seeded such that none passed through the region occupied by the realistic electrode. DBS electrode contacts were numbered in ascending order from the electrode closest to the tip (electrode 0) to the electrode farthest away from the tip (electrode 3). Stimulation geometries included three monopolar configurations (electrodes 0, 1, 2) and one bipolar configuration (electrodes 1, 2). In the bipolar configuration, the active contacts were set to equal amplitudes of opposite polarity.

Zhang and Grill, *J Neural Eng*, 2010

19

## Nerve Stimulation

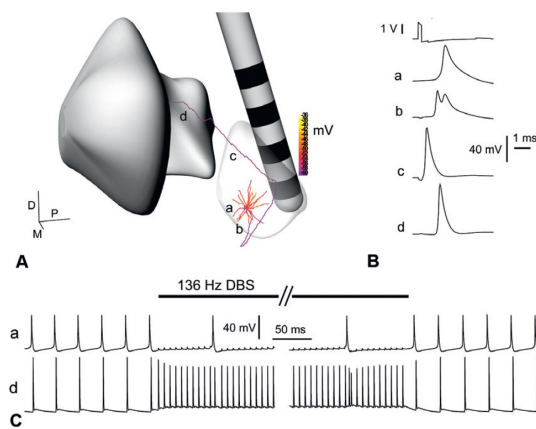


**Fig. 5.2.** Modeling deep brain stimulation (DBS) in the parkinsonian monkey. (A) Three-dimensional (3D) reconstruction of the DBS electrode location in the neuroanatomy (subthalamic nucleus (STN), light gray volume; internal globus pallidus, dark gray volume) and the DBS polarization of a 3D STN neuron model. (B) Lowercase letters indicate location in the STN neuron where the transmembrane voltage was recorded: a, soma; b, first node of Ranvier; c, 30th node of Ranvier; d, 50th node of Ranvier. The action potential initiated in the axon and propagated toward the cell body and axonal terminals in the globus pallidus. The traces in the top row represent the stimulus voltage waveform applied to the neuron. (C) Trains of DBS suppressed somatic firing, but enhanced axonal output. (Adapted from Miocinovic et al., 2006.)

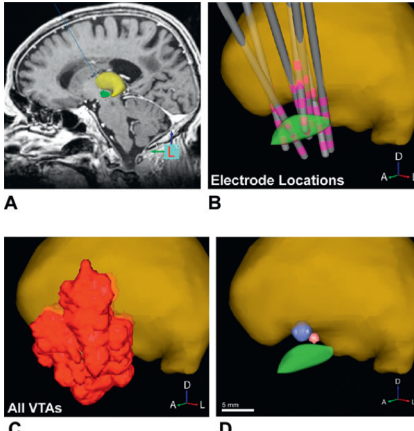
McIntyre and Foutz, *Handb Clin Neurol*, 2013

20

## Patient-Specific DBS Model

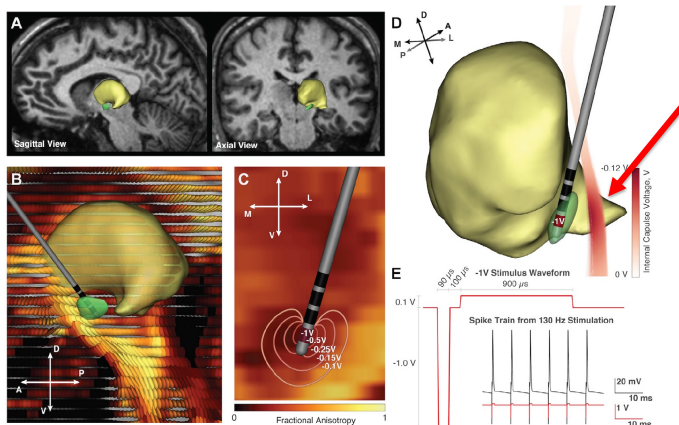
**Fig. 5.3.** Target stimulation volume for Parkinson's disease. (A) Patient-specific model (yellow volume, thalamus; green volume, subthalamic nucleus). (B) Seven different cases of deep brain stimulation (DBS) (28 electrode contact locations all displayed within a common atlas space). (C) Overlay of volumes of tissue activated (VTAs) from 163 different stimulation parameter settings. The combined red volume depicts the total anatomical region mapped by the DBS experiments. All VTAs were overlaid on a 0.5-mm voxelized matrix that encompassed the subthalamic nucleus region. (D) Each VTA had a quantitative clinical outcome score for rigidity and bradykinesia. When a VTA overlapped with a given voxel, its scores were included in the voxel wise statistical analysis. The blue and pink volumes represent voxels that when stimulated generated more than 75% improvement in rigidity or bradykinesia, respectively. (Adapted from Butson et al., 2011.)

McIntyre and Foutz, *Handb Clin Neurol*, 2013



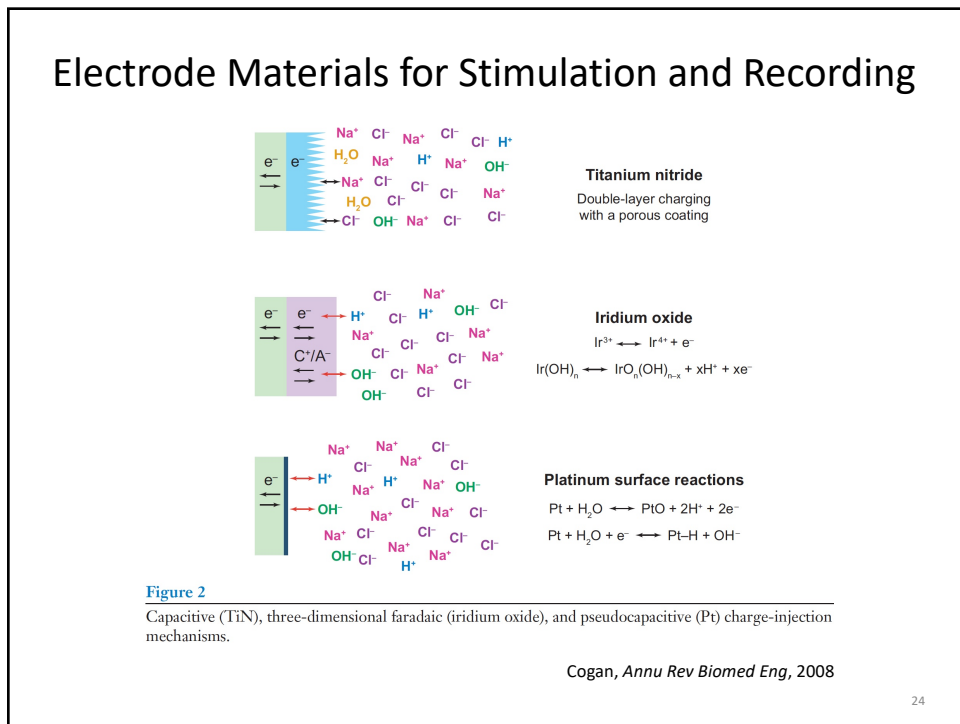
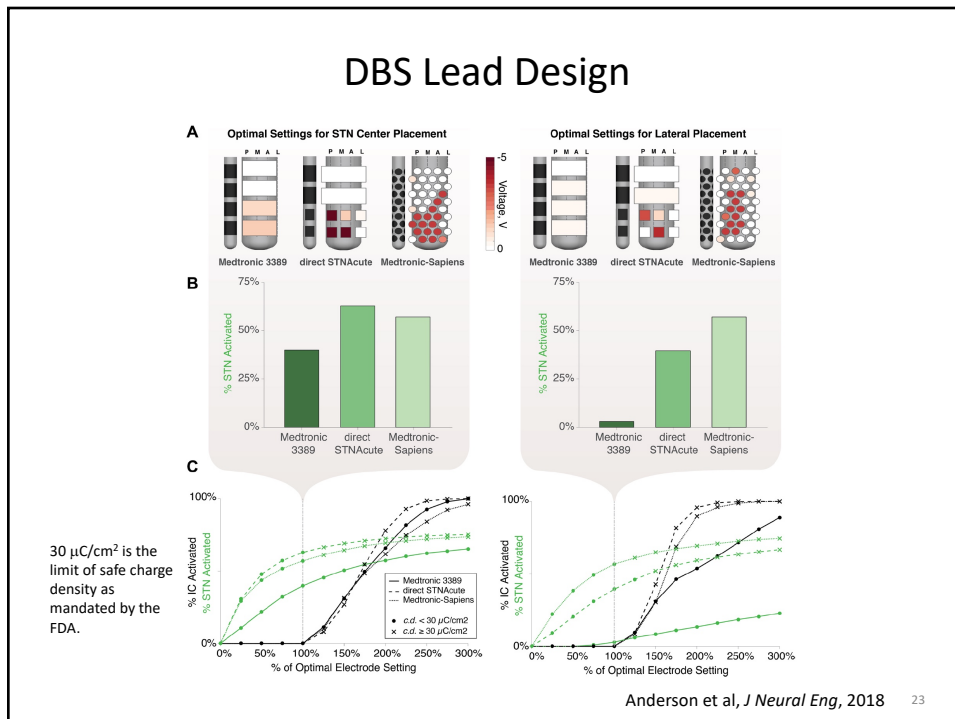
21

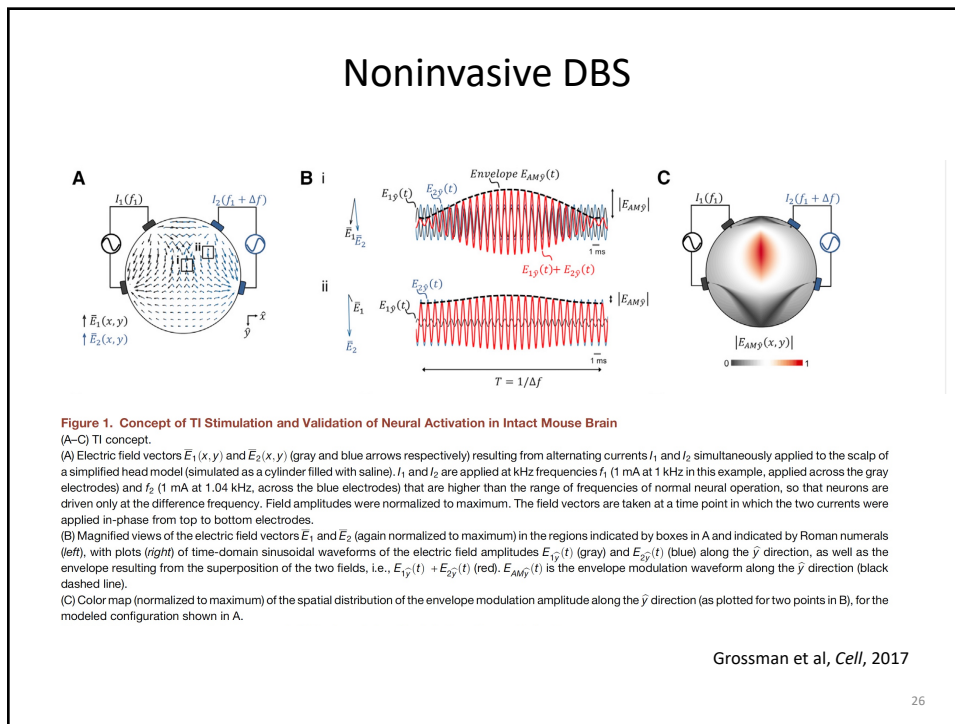
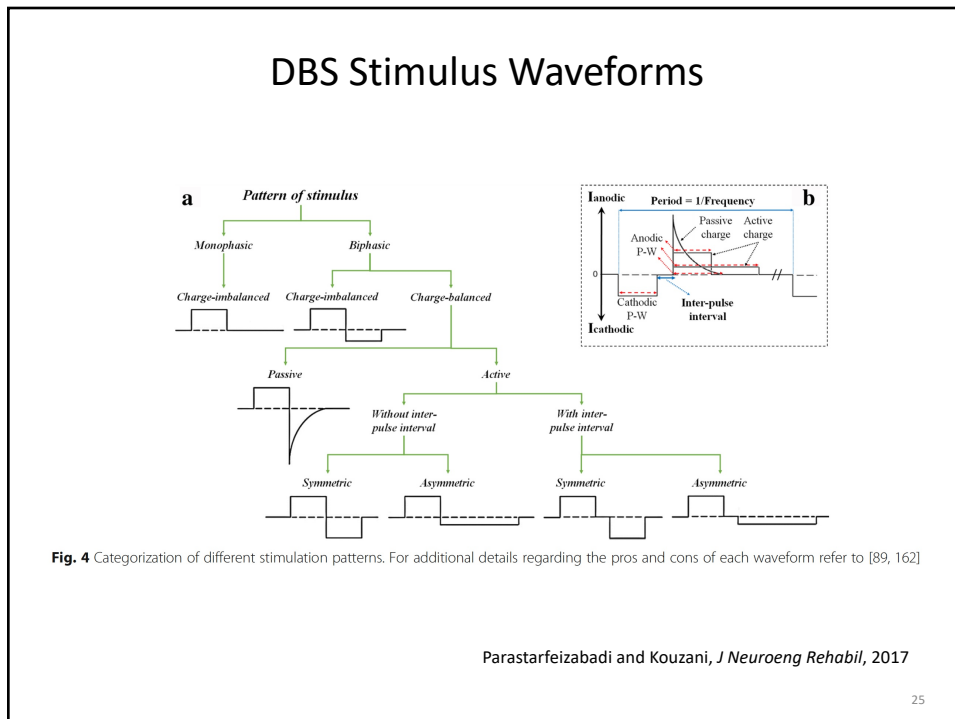
## Patient-Specific DBS Model (Side Effects)



**Figure 2.** Constructing the patient-specific finite element model for a DBS patient for Parkinson's disease with the STN as the target. (A) T1-weighted MRI sagittal and axial slices shown with the segmented STN (green) and thalamus (yellow). (B) A tensor field generated from DTI MRI demonstrates anisotropic flow through brain tissue; yellow coloring indicates high anisotropy while black coloring indicates isotropy. (C) The FEM model incorporates heterogeneous tissue conductivities from DTI MRI to capture anisotropic voltage spread through neighboring brain tissue. (D) Tracts from the IC, containing cortico-motor axons, were generated from a seed region placed laterally from the STN. A total of 708 IC trajectories were generated from diffusion tensors shown in panel B and had a minimum fractional anisotropy value of 0.15. (E) Multi-compartment cable models were solved for each IC trajectory to quantify activation by optimized settings produced by the algorithm. The stimulus waveform consists of a  $90\ \mu s$  cathodic pulse, followed by a  $100\ \mu s$  delay, then a  $900\ \mu s$  anode pulse at 10% of the cathodic voltage. An example spike train can be seen for 130 Hz stimulation at  $-1\text{ V}$ .

Anderson et al, *J Neural Eng*, 2018 22





**190307 Slide Notes****Slide 3. Understanding therapeutic merits of DBS in Parkinsonian neural networks**

From lecture by Dr. Sri Sarma.

**Slide 4. DBS Lead Placement**

Lewis PM, Thomson RH, Rosenfeld JV, Fitzgerald PB. Brain neuromodulation techniques: a review. *Neuroscientist*. 2016;22:406-421

**Slide 5. Selective motor processing in PD under DBS**

From lecture by Dr. Sri Sarma.

**Slide 6. DBS Electrode (Medtronic 338)**

<http://www.medicalexpo.com/prod/medtronic/product-70691-503210.html>

The Lead model 3389 from Medtronic is 40 cm in length and is used specifically for deep brain stimulation. The firm tungsten stylet of the Lead model 3389 provides accurate targeting and placement. The Lead model 3389 is provided with a soft, blunt tip for smooth passage through tissue and a burr hole ring and cap for secure anchoring. The Lead model 3389 kit from Medtronic comes with quadripolar lead, tunneling rod, tunneling rod tip, lead end cap, torque wrench, 2 passing straw, depth stop gauge, short stylet, screening cable model 3550-03 (TwistLock), screening cable model 3550-07 (alligator clips), burr hole cap, burr hole ring, Boot (for percutaneous extension) and StimLoc® lead anchoring device, which comes with lead clip (Cam), entering tool, frame clip insertion tool, disposable screwdriver, burr hole ring, final cap/Burr hole cover and a disposable screwdriver.

The lead contains four active, concentric electrodes, numbered 0-3.

**Slide 7. Active Electrodes**

Yousif N, Liu X. Modeling the current distribution across the depth electrode-brain interface in deep brain stimulation. *Expert Rev Med Devices*. 2007;4:623-631

**Slide 8. Equipotential Surfaces and Current Flowlines**

<http://hyperphysics.phy-astr.gsu.edu/hbase/electric/equipot.html>

**Slide 9. Potential Field from DBS Electrodes**

Miocinovic S, Lempka SF, Russo GS, Maks CB, Butson CR, Sakaie KE, Vitek JL, McIntyre CC. Experimental and theoretical characterization of the voltage distribution generated by deep brain stimulation. *Exp Neurol*. 2009;216:166-176

**Slide 10. Voltage Drop from DBS Electrode Interface**

Chaturvedi A, Butson CR, Lempka SF, Cooper SE, McIntyre CC. Patient-specific models of deep brain stimulation: influence of field model complexity on neural activation predictions. *Brain Stimul*. 2010;3:65-67

**Slide 11. DBS Lead Placement**

Herrington TM, Cheng JJ, Eskandar EN. Mechanisms of deep brain stimulation. *J Neurophysiol*. 2016;115:19-38

**Slide 12. DBS Lead Placement**

McIntyre CC, Chaturvedi A, Shamir RR, Lempka SF. Engineering the next generation of clinical deep brain stimulation technology. *Brain Stimul*. 2015;8:21-26

**Slide 13. DBS Lead Design**

Anderson DN, Osting B, Vorwerk J, Dorval AD, Butson CR. Optimized programming algorithm for cylindrical and directional deep brain stimulation electrodes. *J Neural Eng*. 2018;15:026005

**Slide 14. Electrode Current "Steering"**

Kuhn AA, Volkmann J. Innovations in deep brain stimulation methodology. *Mov Disord*. 2017;32:11-19

**Slide 15. DBS Lead Placement**

Miocinovic S, Somayajula S, Chitnis S, Vitek JL. History, applications, and mechanisms of deep brain stimulation. *JAMA Neurol*. 2013;70:163-171

Placement errors can occur in >40% of implantations (Anderson et al, 2018).

**Slide 16. Cathodal and Anodal Stimulation**

Lewis PM, Thomson RH, Rosenfeld JV, Fitzgerald PB. Brain neuromodulation techniques: a review. *Neuroscientist*. 2016;22:406-421

**Slide 17. Unmyelinated and Myelinated Axons**

Rattay F. Analysis of models for external stimulation of axons. *IEEE Trans Biomed Eng*. 1986;33:974-977

**Slide 18. Nerve Fiber Model**

McIntyre CC, Richardson AG, Grill WM. Modeling the excitability of mammalian nerve fibers: influence of afterpotentials on the recovery cycle. *J Neurophysiol*. 2002;87:995-1006

**Slide 19. Nerve Stimulation**

Zhang TC, Grill WM. Modeling deep brain stimulation: point source approximation versus realistic representation of the electrode. *J Neural Eng*. 2010;7:066009

**Slide 20. Nerve Stimulation**

McIntyre CC, Foutz TJ. Computational modeling of deep brain stimulation. *Handb Clin Neurol*. 2013;116:55-61

**Slide 21. Patient-Specific DBS Model**

McIntyre CC, Foutz TJ. Computational modeling of deep brain stimulation. *Handb Clin Neurol*. 2013;116:55-61

**Slide 22. Patient-Specific DBS Model (Side Effects)**

Anderson DN, Osting B, Vorwerk J, Dorval AD, Butson CR. Optimized programming algorithm for cylindrical and directional deep brain stimulation electrodes. *J Neural Eng*. 2018;15:026005

IC contains cortico-motor neurons. Stimulation of these neurons can produce unwanted side effects, such as side effects such as tonic muscular contraction, dysarthria (difficulty in speaking), conjugate eye deviation (both eyes are turned to the same side as a result of either paralysis or muscular spasms), paraesthesia (an abnormal sensation, typically tingling or pricking ("pins and needles"), caused chiefly by pressure on or damage to peripheral nerves) or gait imbalance (Pollo et al, 2014).

**Slide 23. DBS Lead Design**

Anderson DN, Osting B, Vorwerk J, Dorval AD, Butson CR. Optimized programming algorithm for cylindrical and directional deep brain stimulation electrodes. *J Neural Eng*. 2018;15:026005

**Figure 4.** Validation of algorithm-determined optimal settings. (A) 2D visualizations to show active contacts for the STN center and lateral positions; coloring is based on voltage amplitude. (B) Directional leads were able to activate over 50% of the STN compared to the Medtronic 3389 for the center placement. The direct STNAcute activated more STN than the Medtronic-Sapiens, potentially due to the favorable orientation of the directional contacts; only one column of directional contacts faces the IC. For the lateral placement, the Medtronic-Sapiens electrode was able to activate a similar STN volume as in the centrally placed lead case while the other leads experienced reduced STN activation, especially for the Medtronic 3389 at 2.9%. (C) Contacts were ramped in amplitude to verify that the algorithm produces optimal settings given the constraints used. Lowering the amplitudes results in less STN activation, but increasing the amplitudes past optimal elicits IC activation. Data points represented by an 'x' notation mean the contact configuration exceeds safe charge density limits.

**Slide 24. Electrode Materials for Stimulation and Recording**

Cogan SF. Neural stimulation and recording electrodes. *Annu Rev Biomed Eng*. 2008;10:275-309

Capacitive charging can be either electrostatic, involving purely double-layer ion-electron charge separation and electrolyte dipole orientation, or electrolytic, involving charge stored across a thin, high-dielectric-constant oxide at the electrode-electrolyte interface. Faradaic reactions involve the transfer of an electron across the electrode-electrolyte interface and require that some species, on the surface of the electrode or in solution, undergo a change in valence, i.e., are oxidized or reduced. For noble metal electrodes, primarily Pt and PtIr alloys, the faradaic reactions are confined to a surface monolayer, and these reactions are often described as pseudocapacitive, although electron transfer across the interface still occurs. Charge can also be stored and injected into tissue from valence changes in multivalent electrode coatings that undergo reversible reduction-oxidation (redox) reactions. These coatings, which are typified by iridium oxide, but include newer materials such as poly(ethylenedioxythiophene), are mixed conductors, exhibiting both electron and ion transport within the bulk of the coating.

**Slide 25. DBS Stimulus Waveforms**

Parastarfeizabadi M, Kouzani AZ. Advances in closed-loop deep brain stimulation devices. *J Neuroeng Rehabil*. 2017;14:79  
89. Sooksood K, Stieglitz T, Ortmanns M. An active approach for charge balancing in functional electrical stimulation. *IEEE Trans Biomed Circuits Syst*. 2010;4:162-70.

162. D. R. Merrill, M. Bikson, and J. G. Jefferys, "Electrical stimulation of excitable tissue: design of efficacious and safe protocols," *J Neurosci Methods*, vol. 141, pp. 171-198, Feb 15 2005.

**Slide 26. Noninvasive DBS**

Grossman N, Bono D, Dedic N, Kodandaramaiah SB, Rudenko A, Suk HJ, Cassara AM, Neufeld E, Kuster N, Tsai LH, Pascual-Leone A, Boyden ES. Noninvasive deep brain stimulation via temporally interfering electric fields. *Cell*. 2017;169:1029-1041 e1016